FINAL TECHNICAL REPORT

USGS AWARD G14AP00033

Earthquake rupture propagation into creeping areas of the San Andreas Fault

Principal Investigator: Nadia Lapusta, California Institute of Technology
1200 E. California Blvd., Pasadena, CA 91125
(626) 395-2277, Fax: (626) 568-2719, lapusta@caltech.edu

Abstract

Faults experience both slow slip and fast, seismic-wave producing, rupture events perceived as earthquakes. These behaviors are often assumed to be separated in space and to occur on two different types of fault segments: one with stable, rate-strengthening, friction and the other with rate-weakening friction that leads to stick-slip. The unexpected Mw 9.0 2011 Tohoku-Oki earthquake shook such assumptions by accumulating its largest seismic slip in the area that had been assumed to be creeping. Our group has been developing models in which stable, rate-strengthening behavior at low slip rates is combined with coseismic weakening, allowing unstable slip to occur in segments which can also creep between events. With model parameters based on laboratory measurements on samples from the fault of the Mw 7.6 1999 Chi-Chi earthquake, the long-term slip behavior of the model - examined using the state-of-the-art numerical approach that includes all wave effects - reproduces and explains a number of both long-term and coseismic observations about faults that hosted the Tohoku-Oki and Chi-Chi earthquakes. The implication that earthquake rupture may break through large portions of creeping segments - currently perceived as barriers - requires re-evaluation of seismic hazard in many areas, including California.

In this project, we have investigated the possibility that large earthquakes penetrate below the seismogenic zone (as defined through microseismicity distribution), into the deeper, creeping fault extensions. Our modeling efforts indeed support such a scenario, further indicating that such deeper penetration in past events can be detected by the absence of concentrated microseismicity at the bottom of the seismogenic zone. We have been building a model of such deeper penetration of large events based on thermally induced pressurization of pore fluids, and examining its implications for the microseismicity, interseismic creep, and long-term behavior of the San Andreas Fault (SAF).

We have also started to examine the effect of penetration of seismic slip into creeping areas on the source properties and interaction of repeating sequences. In simplified 2D models with 1D faults, we find that the interaction of repeating sequences is dominated by the static stress changes due to postseismic slip, opening the possibility of constraining the properties of the creeping region using the observed interaction. A more faithful 3D model of the interaction is under construction. To model all these phenomena while producing realistic behavior that can be compared to observations, we use the modeling approach that fully reproduces the inertial, stress-concentrating, effects during seismic events, while seamlessly resolving the transition between seismic and aseismic slip.

The studies have advanced our understanding of the friction properties of the SAF and the penetration depth of large events, which will contribute to the evaluation of seismic hazard in California and other areas. The resulting better understanding of seismic hazard and physics of large destructive events will contribute to reduction of losses from earthquakes in the US. The research is well aligned with the USGS Priority Topics in Research on Earthquake Physics.

Publications and presentations on research supported by this project:

Jiang, J., and N. Lapusta, Deeper penetration of large earthquakes on seismically quiescent faults, *Scienc*e, 352, 2016.

Lui, S.K.Y., and N. Lapusta, Repeating microearthquake sequences interact predominantly through postseismic slip, *Nature Comm*, doi: 10.1038/ncomms13020, 2016.

Higgins, N., and N. Lapusta, Numerical Investigation of Earthquake Nucleation on a Laboratory-Scale Heterogeneous Fault with Rate-and-State Friction, *AGU Fall Meeting*, San Francisco, CA, Dec. 2014. (Oral presentation)

Jiang, J., and N. Lapusta, Connecting depths of seismicity, fault locking, and coseismic slip using long-term fault models, *AGU Fall Meeting*, San Francisco, CA, Dec. 2015. (Oral presentation)

Jiang, J., and N. Lapusta, Connecting depths of seismicity, fault locking, and coseismic slip using long-term fault models, *SCEC Annual Meeting*, Palm Springs, CA, Sept. 2015.

Jiang, J., and N. Lapusta, Variability of earthquake slip and arresting depth in fault models with depth-dependent properties, *SSA Annual Meeting*, Pasadena, CA, Apr. 2015.

Jiang, J., and N. Lapusta, Long-term fault behavior at the seismic-aseismic transition: space-time evolution of microseismicity & depth extent of earthquake rupture, *Cargèse Workshop on Earthquake nucleation, triggering and interactions with aseismic processes*, Corsica, France, Nov. 2014. (Oral presentation)

Jiang, J., and N. Lapusta, Long-term fault behavior at the seismic-aseismic transition: space-time evolution of microseismicity and depth extent of earthquake rupture, *SCEC Annual Meeting*, Palm Springs, CA, Sept. 2014.

Lapusta, N. and J. Jiang, Long-term fault slip in models with depth-dependent permeability and shear zone width: depth extent and spatio-temporal complexity of earthquake ruptures, *AGU Fall Meeting*, San Francisco, CA, Dec. 2014. (Invited oral presentation)

Lui, S.K.Y., and N. Lapusta, Modeling the LA and SF repeating sequences in Parkfield, *SSA Annual Meeting*, Pasadena, CA, Apr. 2015. (Oral presentation)

Lui, S.K.Y., and N. Lapusta, Interaction of repeating earthquake sequences and its relation to fault friction properties, *AGU Fall Meeting*, San Francisco, CA, Dec. 2014. (Oral presentation)

Lui, S.K.Y., and N. Lapusta, Interaction of repeating earthquake sequences and its relation to fault friction properties, *2014 Cargèse Workshop on Earthquake nucleation, triggering, and relationship with aseismic processes*, Corsica, France, Nov. 2014. (Oral presentation)

Lui, S.K.Y., and N. Lapusta, Interaction of repeating earthquake sequences and its relation to fault friction properties, *2014 SCEC Annual Meeting,* Palm Springs, CA, Sept. 2014.

1. Physical model for seismic slip in creeping regions

Our model includes two aspects of earthquake source physics that have been gaining acceptance and validation through laboratory experiments and comparison of earthquake models with observations. The first one is the rate-and-state nature of fault friction at low, aseismic slip rates, conclusively documented in laboratory experiments and used to reproduce, both qualitatively and quantitatively, a number of earthquake-source observations (Dieterich, 2007; Scholz, 1998). Our previous studies supported by USGS have shown that the standard logarithmic rate and state formulations (Dieterich, 1979, 1981; Ruina, 1983; Blanpied et al., 1991, 1995) already allow us to match a number of basic observations

regarding the Parkfield segment behavior (Chen and Lapusta, 2009; Chen et al., 2010; Barbot et al., 2012). Such laws express the dependence of frictional shear strength τ_f on the effective normal stress $\bar{\sigma}$, slip rate V (which we also call slip velocity), and evolving properties (state) of the contact population represented by the state variable θ, through:

$$\tau_f = \bar{\sigma} f = (\sigma - p)[f_o + a \ln(V / V_o) + b \ln(V_o \theta / L)],$$
$$\frac{\partial \theta}{\partial t} = 1 - \frac{V\theta}{L} \text{ or } \frac{\partial \theta}{\partial t} = -\frac{V\theta}{L} \ln \frac{V\theta}{L} \text{ or } \frac{\partial \theta}{\partial t} = \exp\left(-\frac{V}{V_c}\right) - \frac{V\theta}{L} \ln \frac{V\theta}{L}, \tag{1.1}$$

where σ is the normal traction, p is the pore pressure, f_o, V_o, a, b, and L are rate and state parameters, with L being the characteristic slip for state variable evolution, and V_c is the cut-off velocity of the order of 10^{-8} m/s. In these laws, the rate and state features result in small variations (of the order of 1-10%) from the baseline frictional strength given by $\bar{\sigma} f_o$. Despite being small, these variations are fundamentally important for physically and mathematically meaningful stability properties of frictional sliding (e.g., Rice, Lapusta, and Ranjith, 2001). In the steady state, $(a - b)$ is the rate-and-state parameter that can be used to model both stable, velocity-strengthening (VS) fault segments ($a - b > 0$) and potentially seismic, velocity-weakening (VW) fault segments ($a - b < 0$).

The second emerging property of the earthquake source is additional substantial fault weakening at seismic slip rates. While theories of such weakening have a long history (Sibson, 1973), relatively recent laboratory confirmations of this phenomenon (Tsutsumi and Shimamoto, 1997; Tullis, 2007) have put this notion on the earthquake science map. Our prior support from USGS and NSF has enabled us to incorporate shear heating dynamic weakening mechanisms, such as flash heating and thermal pressurization, into our simulations of earthquake cycles (e.g., Noda and Lapusta, 2010, 2013). One shear-heating weakening mechanism that has laboratory support is flash heating (e.g., Rice, 1999, Goldsby and Tullis, 2003, Beeler and Tullis, 2003, Rice, 2006, Beeler et al. 2008), in which tips of contacting fault gouge grains heat up and weaken. Such weakening can be activated even for very small slips of the order of 100 microns if the shear strain rate is high enough. Hence this mechanism can be important even for the smallest earthquakes. Another relevant mechanism is pore fluid pressurization (e.g., Sibson, 1973; Andrews, 2002; Noda, 2004; Bizzarri and Cocco, 2006a,b; Rice, 2006; Noda et al., 2009), in which rapid shearing raises the temperature and hence pore fluid pressure, lowering the effective normal stress and hence the frictional resistance. To include flash heating and/or pore pressurization into our models, we modify the logarithmic rate and state formulation (1.1) to

$$\tau_f = \bar{\sigma} f = (\sigma - p)\left[\frac{f_o - f_w + a \ln(V / V_o) + b \ln(V_o \theta / L)}{1 + L / \theta V_w} + f_w\right], \tag{1.2}$$

where V_w is the characteristic slip velocity at which flash heating starts to operate, f_w is the residual friction coefficient, and pore pressure p could be evolving due to shear heating as discussed below. Based on laboratory experiments and flash heating theories, V_w is of the order of 0.1 m/s. Selecting much larger values of V_w than the seismic slip rates of the order of 1-10 m/s would effectively disable the additional weakening due to flash heating. The coupled temperature and pore pressure evolution is calculated by (Rice, 2006 and references therein, Noda et al., 2009, Noda and Lapusta, 2010):

$$\frac{\partial T}{\partial t} = \alpha_{th} \frac{\partial^2 T}{\partial y^2} + \frac{\omega(y)}{\rho c}, \quad \frac{\partial p}{\partial t} = \alpha_{hy} \frac{\partial^2 p}{\partial y^2} + \Lambda \frac{\partial T}{\partial t}, \tag{1.3}$$

where y is the space coordinate normal to the fault, T is the temperature, α_{th} and α_{th} are the thermal and hydraulic diffusivities, $\omega(y)$ is the heat generation rate the integral of which over the width w of the shearing layer equals to $\tau_f V$, ρc is the specific heat, Λ is pore pressure change per unit temperature change under undrained condition. (Note that this formulation can also include inelastic dilatancy, as an additional term in the equation for the pore pressure evolution.) The heat source, $\omega(y)$, is distributed in a narrow shear zone around the fault. The standard assumption is to take this term to represent the effect of uniform sliding in the fault zone of thickness w.

In our simulations, spontaneous long-term slip history of fault slip is determined using the 3D simulation methodology of Lapusta and Liu (2009) and Noda and Lapusta (2010), which is the extension of the 2D methodology of Lapusta et al. (2000). The methodology incorporates slow tectonic-type loading and all dynamic effects of self-driven dynamic rupture. The algorithm allows us to treat accurately long deformation histories and to calculate, for each earthquake episode, initially quasi-static accelerating slip (nucleation process), the following dynamic rupture break-out and propagation, postseismic response, and ongoing slippage throughout the loading period in creeping fault region.

2. Depth extent of large earthquakes on mature strike-slip faults

We have successfully applied this paradigm to exploring the possibility of deeper slip in large earthquakes. It is typically assumed that all seismic slip is confined within the seismogenic zone - often defined by the extent of the background seismicity - with regions below creeping. In terms of rate-and-state friction properties, the locked seismogenic zone and the deeper creeping fault extensions are velocity-weakening (VW) and velocity-strengthening (VS), respectively. Recent studies have suggested that earthquake rupture could penetrate into the deeper creeping regions (Shaw and Wesnousky, 2008), and yet deep slip is difficult to detect due to limited resolution of source inversions with depth.

Our study has shown that the absence of concentrated microseismicity at the bottom of the seismogenic zone may point to the existence of deep-penetrating earthquake ruptures (Jiang and Lapusta, 2015; 2016). The creeping-locked boundary creates strain and stress concentrations. If it is at the bottom of the VW region, which supports earthquake nucleation, microseismicity should persistently occur at the bottom of the seismogenic zone. Such behavior has been observed, e.g. on the Parkfield segment of the San Andreas Fault (SAF) and the Calaveras fault (Figures 1A and 1B, Waldhauser et al., 2004, Rubinstein and Beroza, 2007). However, such microseismicity is inhibited if dynamic earthquake rupture penetrates substantially below the VW/VS transition, dropping stress in the ruptured VS areas and making them effectively locked. Hence the creeping-locked boundary, with its stress concentration, is located within the VS area, where earthquake nucleation is inhibited. Indeed, microseismicity concentration at the bottom of the seismogenic zone is not observed for several faults that hosted major earthquakes, such as the Carrizo and Coachella segments of the SAF (Figure 1c) and the Denali fault (Ratchkovski et al, 2003).

We have confirmed this hypothesis by simulations that adopt the kind of modeling described in section 1 to this problem (Figure 2; Jiang and Lapusta, 2016). In our model, a VW region is surrounded by VS areas. Around the deeper transition from the VW to VS behavior, patches of smaller nucleation sizes are added to simulate fault heterogeneity that could lead to microseismicity. Such patches are likely present shallower as well but we do not include them in the model for numerical efficiency, since we focus on the behavior at the transition. Thermally-induced pore fluid pressurization (TP) is effective on a part of the fault, leading to enhanced coseismic weakening. In the case where efficient TP is restricted to the VW zone, model-spanning earthquakes arrest quickly in the VS areas, and the creeping-locked boundary reaches the bottom of the VW region early in the earthquake cycle, producing microseismicity (Figure 2, panels A1, B1, C1). In contrast, if efficient TP extends deeper (5 km deeper in the example), earthquake rupture activates coseismic weakening in the VS areas, penetrating much deeper and

generating larger average slip (Figure 2, panels A2, B2). In this case, the creeping-locked boundary, while moving up-dip with time (Figure 2, panel D2), is below the VW area throughout the interseismic period, producing essentially no microseismicity (Figure 2, panel C2).

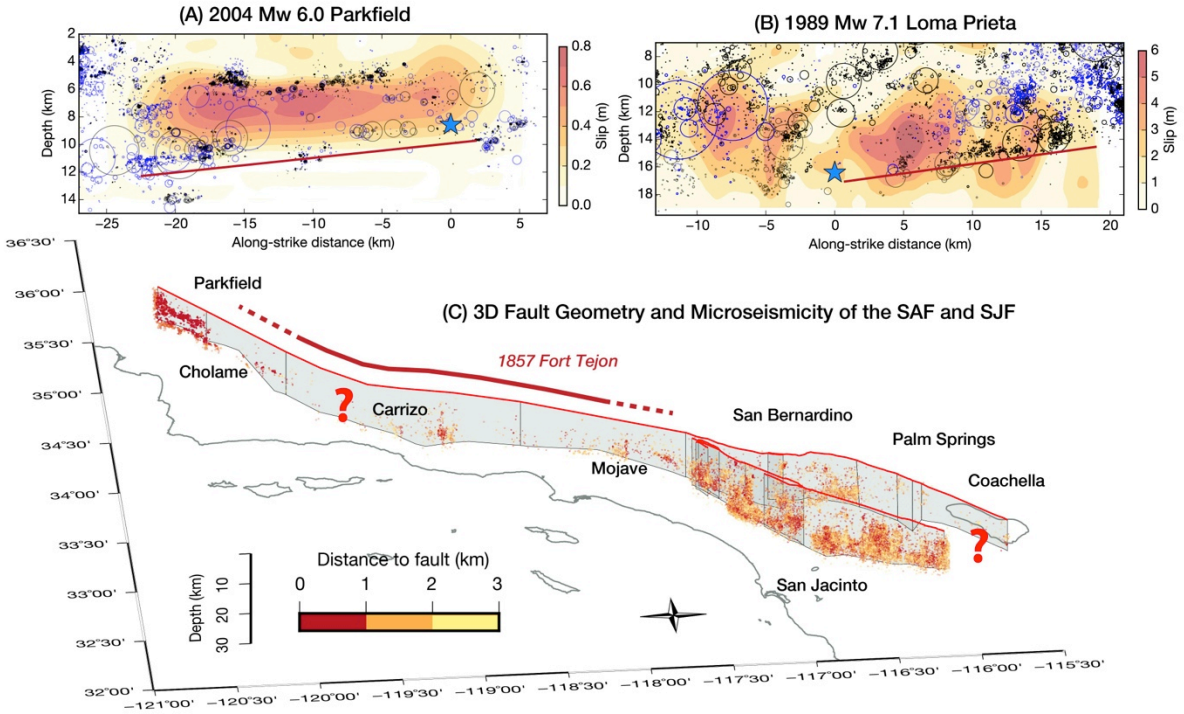

Figure 1. **Examples of the relation between seismicity and slip in large events.** 20-year seismicity prior to the mainshock (blue), 5-year aftershocks (black) (from NCSN catalogue; Waldhauser and Schaff, 2008) and estimated earthquake slip (in color) for (A) 2004 Mw 6.0 Parkfield earthquake and (B) 1989 Mw 7.1 Loma Prieta earthquake. Slip models are from Barbot et al. (2012) and Beroza (1991), respectively. Red lines mark the alignment of microseismicity at the creeping-locked boundary. Blue stars are earthquake hypocenters. (C) Seismicity in Southern California (1981-2011) within 3 km to either SAF or SJF (Hauksson, 2012). Fault geometries are from the SCEC Community Fault Model; the vertical scale is exaggerated to emphasize the fault depth. Active seismicity at depth is observed for San Jacinto fault, Parkfield segment and San Bernardino segment of San Andreas fault; Cholame, Carrizo and Coachella segments with major events in the past (including the 1857 Fort Tejon earthquake with inferred extent indicated by the solid-dashed red line) have been seismically quiet for decades, including no to little seismicity at the bottom of the seismogenic zone.

Hence the absence of concentrated microseismicity at the bottom of the seismogenic zone likely points to deeper penetration of large earthquakes. The relation between the microseismicity and depth of slip in large earthquakes can help us understand historical events and evaluate potential future earthquake scenarios on mature strike-slip fault segments, including those of the SAF. The 1857 M_w 7.9 Fort Tejon earthquake is the last major event on the San Andreas/San Jacinto fault system in Southern California (Hauksson, 2012; Fig. 3) which ruptured the Cholame, Carrizo, and Mojave segments (Bouchon and Karabulut, 2008; Sieh, 1978). Deeper penetration of these two segments are supported by the report of deep slip of ~11m and 16 m inferred from historical surveys, despite lower slip at the surface of 3-6 m and 5 m, respectively (Smith-Konter et al., 2011; Grant et al., 1994). The last major earthquake on the Coachella segment occurred in ~1690 and potentially also ruptured the San Bernardino and Palm Springs segments (Fialko, 2006). The recurrence of such events pose severe seismic risk for Southern California. Virtually no microseismicity is currently observed on all these segments (Fig. 1).

In the light of our modeling, this observation implies that, ~150 to ~300 years after the previous major seismic events, the locked-creeping transition on those segments is still below the bottom of the seismogenic zone. To achieve that, dynamic rupture on those segments should have penetrated an additional depth below the seismogenic zone, at least 3-5 km based on our estimates derived in section 3, and perhaps much more. Interseismic geodetic observations indeed suggest that the Carrizo and Coachella segments are accumulating more potency deficit than other fault segments, which they are expected to release in future events (Zielke et al., 2010).

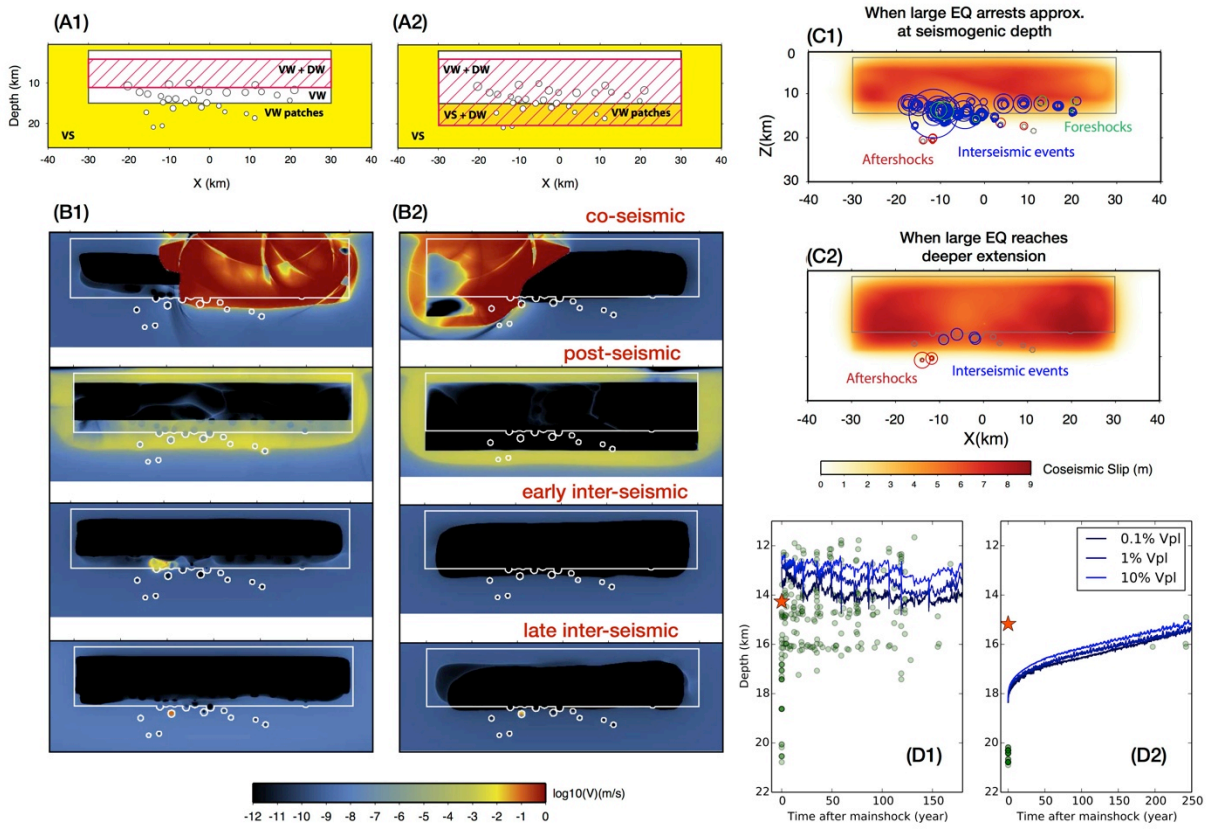

Figure 2. Dynamic fault models that reproduce the observed behavior of microseismicity (Figure 1) and suggest the possibility of deeper penetration of large earthquakes. Two models are compared with different spatial extent of enhanced dynamic weakening (DW) with respect to the VW region at low slip rates: (A1) Model M1 with DW (red hashed region) confined within the VW region (white) and (A2) Model M2 with DW extending into the deeper VS region (yellow). Patches of smaller nucleation sizes are added to the model at the transitional depths (grey circles) to explore the effect of the stress concentration there on seismicity. (B) Slip rate snapshots for typical large earthquakes out of sequences simulated and their aftermath. Earthquakes penetrate deeper in model M2, with stress concentration between the locked (black) and deeper creeping (blue) fault areas located below most of the VW region capable of earthquake nucleation (except for some imposed small patches). (C) Spatial patterns of microseismicity in relation to earthquake slip (in color). Events are illustrated using a circular crack model with equivalent seismic moment and stress drop of 3 MPa. Note the microseismicity streaks in model M1 and their near absence in model M2. (D) Time evolution of locking depths defined as the depths with slip rates of 0.1%, 1% and 10% of the plate rate (blue lines) and seismicity depth (green dots) during one post- and inter-seismic period. Red stars give the locking depths prior to the mainshock.

3. Estimating the upward migration of the stress concentration front

When earthquake rupture penetrates below the seismogenic zone (VW region), the stress concentration front (SCF) induced at the locked-creeping transition (LCT) is within the VS region, and migrates up dip due to gradual resumption of creep in the post- and inter- seismic periods. Therefore, the depth of the SCF in the interseismic period is connected to the depth extent of (previous) coseismic slip.

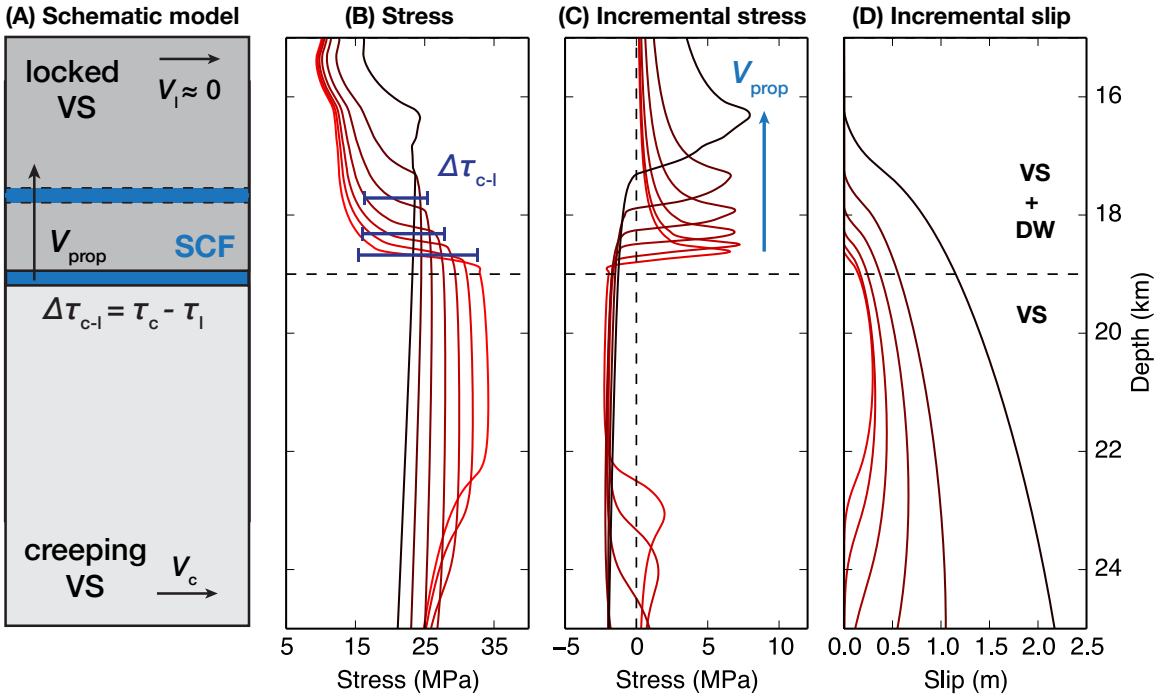

Figure 3: Post- and inter-seismic migration of the stress concentration front (SCF) after a deeper-penetrating earthquake. (**A**) Schematics of SCF (blue strips) advancing up dip with a (time-dependent) propagation speed V_{prop}. The locked and creeping VS regions are associated with slip rates $V_l(\approx 0)$ and V_c, and shear stresses τ_l and τ_c, respectively. The difference of stress across SCF is $\Delta\tau_{c\text{-}l}$. (**B**) Depth profiles of shear stress during the post- and inter-seismic periods (from red to black: 30 min, 5 hours, 2, 20, 200 days, 5 and 50 years), similar to Fig. S17. $\Delta\tau_{c\text{-}l}$ for different times are marked. (**C**) Incremental stress and (**D**) incremental slip during the time intervals shown in (B), suggest a quasi-static, slowly expanding crack. The stress peaks in (C) indicate approximate locations of the SCF. The horizontal dashed lines mark the transitions between VS+DW and VS regions. The vertical dashed line indicates no stress change.

As illustrated in Fig. 3(A), the SCF moves up dip with time, separating locked and creeping regions. The coseismically ruptured region gets loaded while stress decays in the unruptured region due to postseismic slip. Let us denote the difference between the stress levels across the SCF by $\Delta\tau_{c\text{-}l}$. In Fig. 3 (C-D), the incremental stress and slip over several consecutive time periods indicate that this process is similar to a 2D (Mode III) antiplane quasi-static crack that slowly advances into the locked region, with time-dependent creeping rates and stress concentration in front of the crack tip. Based on kinematics, the propagation speed of the SCF is equal to the spatial slip gradient (right behind the tip) times maximum slip rate at the SCF. Since slip gradient, as shear strain, is related to stress difference via shear modulus μ, and maximum slip rate at the SCF is just the creeping rate $V_c(t)$, we arrive at the following expression:

$$V_{\text{prop}}(t) = \alpha \mu \frac{V_{\text{c}}(t)}{\Delta\tau_{\text{c-l}}(t)} \tag{3.1}$$

where α is a coefficient to account for geometrical effects of mapping our results into this approximate model, $\Delta\tau_{\text{c-l}}(t)$ is the stress difference across SCF, and t is the time since the previous large earthquake. $\Delta\tau_{\text{c-l}}(t)$ is affected by several processes and can be written as:

$$\Delta\tau_{\text{c-l}}(t) = \tau_{\text{c}}(t) - \tau_{\text{l}}(t) = \tau_{\text{c}}(t) - [\tau_{\text{c}}(0^-) + \Delta\tau + \Delta\tau_{\text{load}}(t)], \tag{3.2}$$

where $\tau_{\text{c}}(t)$ and $\tau_{\text{l}}(t)$ are the stresses in the creeping and locked regions at time t, respectively, $t = 0^-$ is the time right before the earthquake, $\Delta\tau$ is coseismic stress increase, and $\Delta\tau_{\text{load}}$ is the stress increase from loading. $\Delta\tau$ is comparable to the static stress drop during the earthquake $\Delta\tau_{\text{eq}}(<0)$, so we assume $\Delta\tau = -\Delta\tau_{\text{eq}} > 0$.

To use Eq. (3.1), we need an estimate of $V_{\text{c}}(t)$ and $\tau_{\text{c}}(t)$. In the VS region below the seismogenic zone, postseismic afterslip following large events has been amply documented, e.g., (Reilinger et al., 2000; Day et al., 2005). These observations can be well explained with steady-state VS friction, at least for periods after tens of days since the event, as supported by numerical studies (Tullis, 2007; Tanikawa, 2009). Hence we can write:

$$\tau_{\text{c}}(t) = \bar{\sigma}\left[f^* + a\log(V_{\text{c}}(t)/V^*)\right] \tag{3.3}$$

Note that we have simplified the notations by using only rate-and-state parameter a since $b = 0$ for the deeper fault extensions in our models. When $b \neq 0$, a is replaced by $(a-b)$ in Eq. (3.3). Formulations for steady-state postseismic fault slip are derived in (Tullis, 2007) with a spring-slider analog. The spring-slider (SS) model ignores the time variation in the size and properties of the afterslip fault zone, but may provide a simplified description of our results. In the context of earthquake sequences, the loading rate V_0 and the rate before perturbation V_i in their model coincide with the late-interseismic fault slip rate in our models, therefore $V_i = V_0 = V_{\text{c}}(0^-)$. Recognizing that, we express fault slip rate $V_c(t)$, slip $\delta_{\text{c}}(t)$, and stress $\tau_{\text{c}}(t)$ with formulations modified from (Tullis, 2007) as follows:

$$\delta(t) = V_i t_{\text{r}} \log\left[1 + d(\exp(t/t_{\text{r}}) - 1)\right], \tag{3.4}$$

$$V_{\text{c}}(t) = V_i \frac{d\exp(t/t_{\text{r}})}{1 + d(\exp(t/t_{\text{r}}) - 1)}, \tag{3.5}$$

$$\tau_{\text{c}}(t) = \bar{\sigma} f^* + a\log(V_{\text{c}}(t)/V^*), \tag{3.6}$$

with

$$d = \exp(-\Delta\tau_{\text{eq}}/a\bar{\sigma}) = V_{\text{c}}(0^+)/V_{\text{c}}(0^-) \quad \text{and} \quad t_{\text{r}} = a\bar{\sigma}/kV_i = a\bar{\sigma}/\dot{\tau},$$

where t_r is the characteristic time for the postseismic period, k is the spring stiffness in the spring-slider model, and $\dot{\tau}$ is the shear stressing rate. To compare the behavior of our models with the simplified formulation above, we take the values of $a\bar{\sigma}$, recurrence time T_r (~250 yr.), coseismic stress drop $\Delta\tau_{\text{eq}}$ (~10 MPa), and V_i ($0.4 - 0.5 V_{\text{pl}}$) from the 3D models. Using the constraint for total slip, $T_{\text{r}}V_{\text{pl}} = V_i t_{\text{r}} \log(1 + d(\exp(T_{\text{r}}/t_{\text{r}}) - 1))$, we solve for the effective t_r. In Fig. 4, we show the behaviors of

VS regions in three models (model M2-L, M2, M2-H) with different friction properties at depth. The general trend of the postseismic fault response in the VS region of the 3D models is predicted relatively well by Eqs. (3.4)-(3.6) for $t > 10^6$ seconds (10 days) after the event. The increasing deviations with a larger value of a suggest a time-variable t_r in the 3D models due to the expansion of postseismic slipping regions. In the late interseismic period before an event, the VS region slips at a rate below the long-term plate rate, as seen in other studies as an expanding stress-shadowing zone (Mizoguchi, 2008). In the context of our models, such lower rate is needed to balance the afterslip.

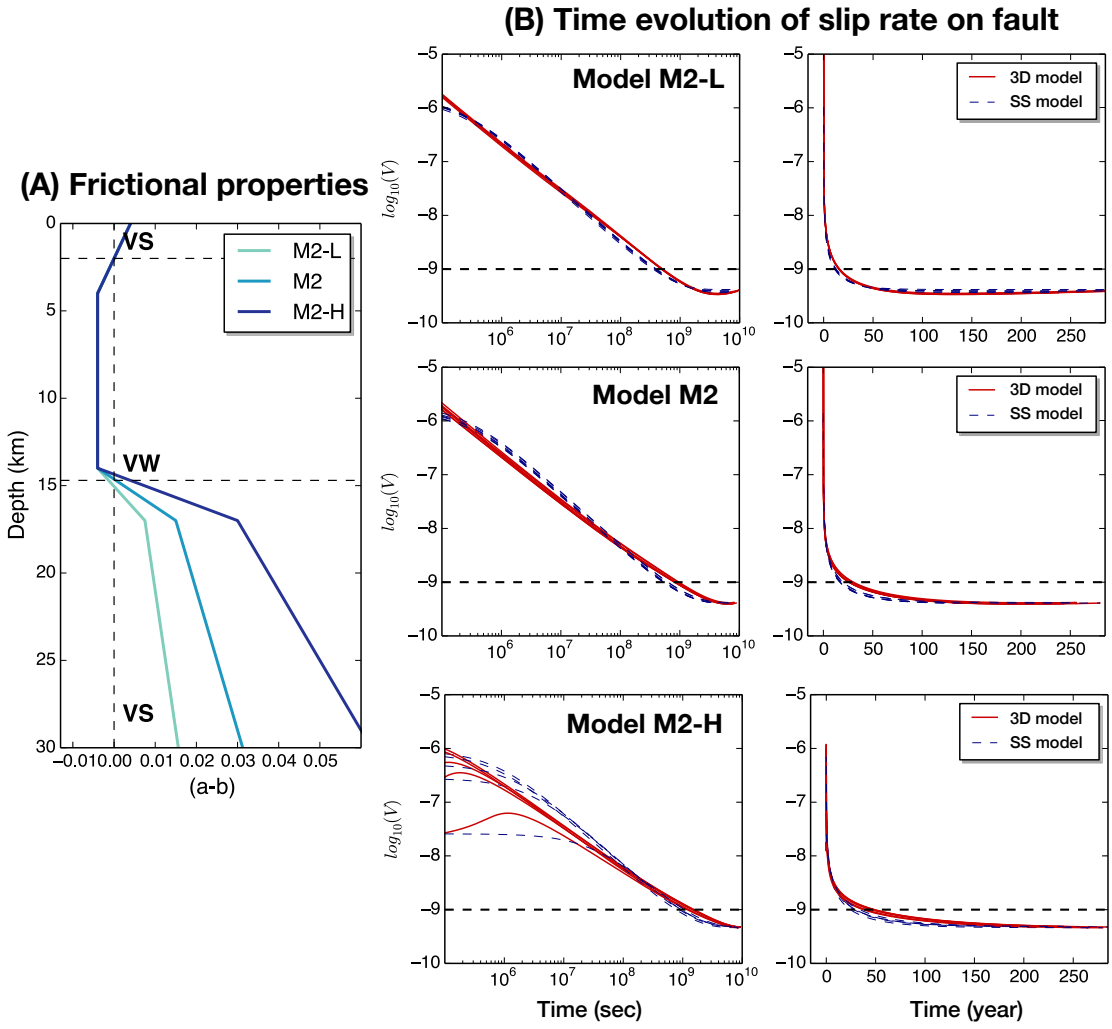

Figure 4: Postseismic response of faults with different frictional properties at depth. (**A**) Depth dependence of frictional properties $(a-b)$ for three models M2-L, M2 and M2-H. (**B**) Postseismic fault slip rates at the depth of 21.5 km ($a-b=$ 0.01, 0.02, 0.04 for the three models, respectively), just below the depth extent of the preceding large earthquake rupture. Numerical results from our 3D models are shown in the red lines and theoretical predictions based on the spring-slider (SS) model (Eq. 13) are shown in blue dashed lines.

Combining Eqs. (3.1), (3.4), (3.5), and (3.6), the migration speed of the SCF in the post- and inter-seismic periods is given as:

$$V_{\text{prop}}(t) = \alpha G \frac{V_{\text{c}}(t)}{\tau_{\text{c}}(t) - \left[\tau_{\text{c}}(0^-) + \Delta\tau_{\text{eq}} + \Delta\tau_{\text{load}}(t)\right]}$$
$$\approx \alpha G\, V_{\text{c}}(t)\left[\bar{\sigma} f^* + a\bar{\sigma}\log(V_{\text{c}}(t)/V^*) - (\tau_{\text{c}}(0^-) + \Delta\tau_{\text{eq}})\right]^{-1},$$

where the pre-seismic stress level for the creeping regions is $\tau_{\text{c}}(0^-) = \bar{\sigma}[\mu^* + a\log(V_i/V^*)]$. We ignore the stressing $\Delta\tau_{\text{load}}(t)$, since this term is smaller compared to other stress changes, and this simplification leads to a lower-bound estimate on V_{prop}. Then we get the following estimate for the migration speed and propagation distance of the SCF:

$$V_{\text{prop}}(t) = \frac{\alpha G\, V_{\text{c}}(t)}{a\sigma\log(V_{\text{c}}(t)/V_i) - \Delta\tau_{\text{eq}}}, \tag{3.7}$$

$$D_{\text{prop}}(t) = \int_0^t V_{\text{prop}}(t')\,\mathrm{d}t' \quad \text{for} \quad t \le T_{\text{r}}. \tag{3.8}$$

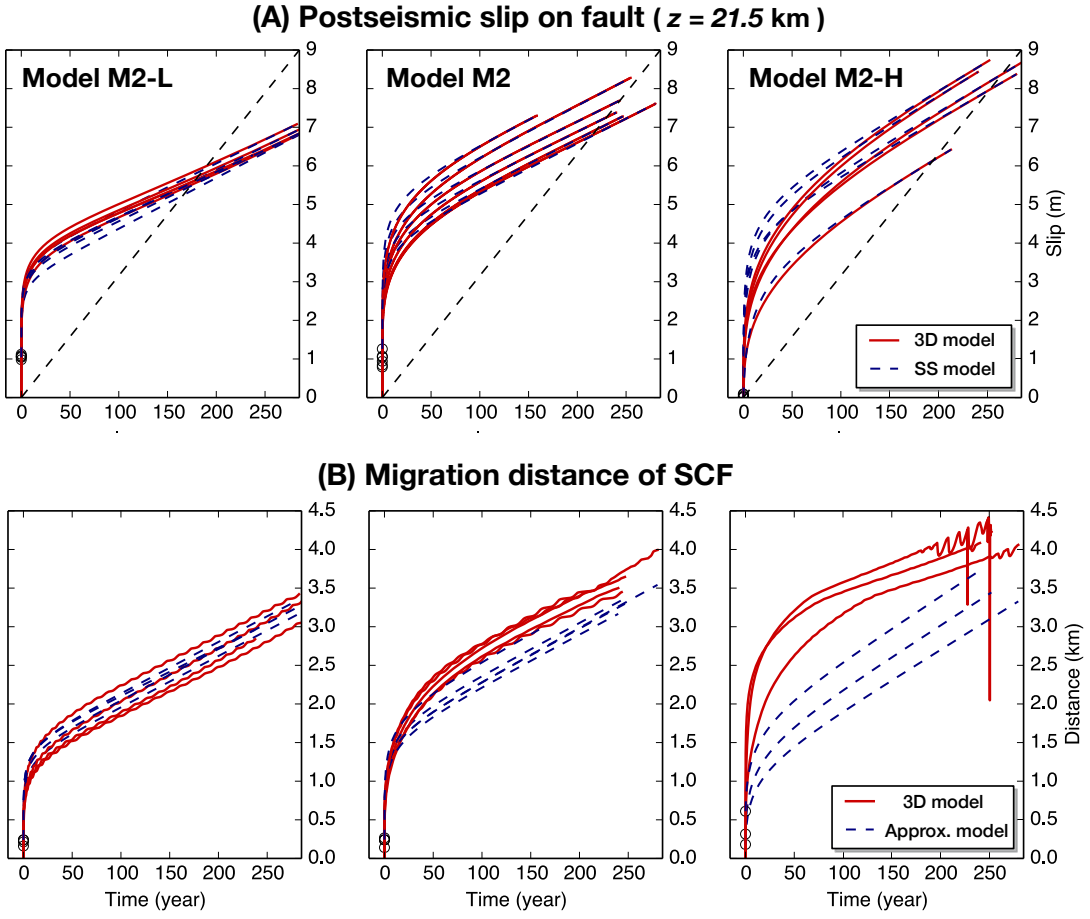

Figure 5: Fault slip and migration of SCF in a post- and inter-seismic period. (**A**) Postseismic fault slip in the VS region ($z = 21.5$ km) in the 3D models and spring-slider (SS) models. The three 3D models have different frictional properties at depth (Fig. 4). (**B**) Migration of the SCF (defined here as the depth with a slip rate of $0.1V_{\text{max}}$, where V_{max} is the maximum slip rate over the fault at the time) in 3D models and its approximation (Eqs. 3.7 - 3.8). We use 10^5 s (~1 day, marked by black circles) after the end of the earthquake as the origin time for the approximate solutions.

Using Eq.(3.7), we find that $\alpha = 0.18$ gives a reasonable match between our 3D fault models and the simplified estimate, with deviations expected for cases with larger $a\bar{\sigma}$ (Fig. 5). Nonetheless, the total migration distance in all models is well reproduced.

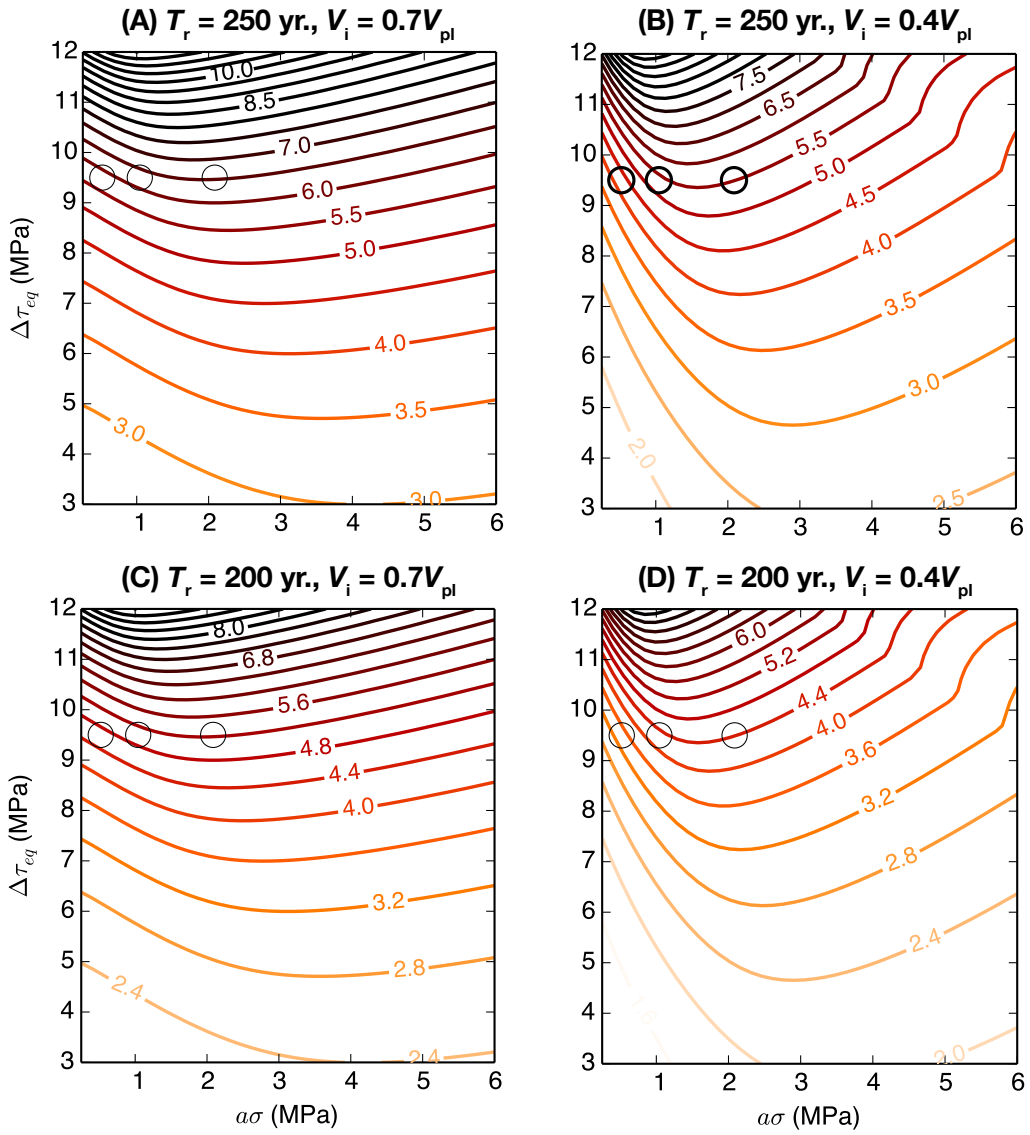

Figure 6: Dependence of migration distance of the SCF D_{prop} on $\Delta\tau_{\text{eq}}$ and $a\bar{\sigma}$. Different combinations of earthquake recurrence time T_{r} (200 and 250 years) and late interseismic fault slip rate V_i ($0.4V_{\text{pl}}$ and $0.7\,V_{\text{pl}}$) are used in the calculation. Black circles (thick lines) indicate the approximate locations in the parameter space for the three models M2-L, M2, and M2-H ($T_{\text{r}} \approx 250$ yr., $V_i \approx 0.4\,V_{\text{pl}}$), and their corresponding locations (thin lines) in other plots.

Using Eq.(3.8), we can estimate the total migration distance of SCF, and hence of the locked-creeping transition, for fault segments with a range of properties, e.g., known T_r and V_{pl} and feasible values for $a\bar{\sigma}$ and $\Delta\tau_{eq}$. In Fig. 6, we make such an estimation for $a = 0.005\text{-}0.03$, $\sigma = 50\text{-}200$ MPa and $\Delta\tau_{eq} = 3\text{-}12$ MPa, assuming different combinations of parameters $V_i = 0.4V_{pl}$ or $0.6V_{pl}$ and $T_r =$ 200 or 250 yr. We observe that D_{prop} depends strongly on $\Delta\tau_{eq}$ and relatively weakly on $a\bar{\sigma}$. In the cases with small $a\bar{\sigma}$, a significant fraction of the postseismic slip occurs in a short time period (t < 10 days) following the event, so the approximate model would under-estimate D_{prop}. In the cases with large $a\bar{\sigma}$, the overall small postseismic slip rate over a large characteristic time would lead to a smaller D_{prop}. Based on these considerations, for events with larger stress drops (> 5 MPa) and reasonable values of $a\bar{\sigma}$, this migration distance could be at least 3-5 km, leading us to conclusions at the end of section 2.

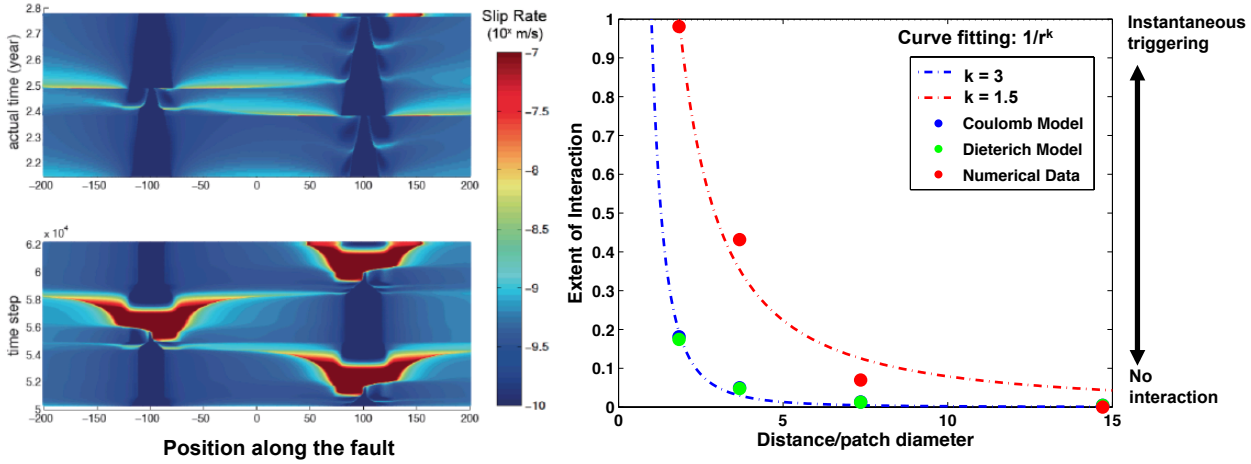

Figure 7. **Interaction of two repeating earthquake sequences in a creeping segment dominated by postseismic slip.** (Left) Slip rate evolution on a 1D fault with two identical VW patches, shown both in actual time (top) and as a function of (variable) time steps to emphasize changes during seismic events and postseismic slip (bottom). Red color includes coseismic rupture. Postseismic creep fronts (PCFs) are clearly visible, traveling from one patch to the other. The PCF from the right patch (at ~2.4 yrs or $5.4\text{x}10^4$ time steps) triggers a seismic event on the left patch (at ~ 2.5 yrs). The PCF from the left patch only triggers aseismic slip on the right patch (at ~2.65 yrs), because the patch is far from failure. (Right) Two-patch interaction in our simulations (red circles) vs. the separation distance between the patches. 1 and 0 correspond to instantaneous triggering and no interaction, respectively. Blue and green circles are theoretical estimates of the interaction because of static stress changes experienced by one of the patches due to coseismic slip on the other patch. At separation distances less than five patch diameters, the significant difference between numerical results and theoretical estimates is mostly contributed by stress changes due to propagating postseismic slip. Postseismic slip also causes the interaction of the two patches to extend much farther than the typically expected distances of one to two patch diameters.

4. Interaction of small repeating earthquakes dominated by postseismic slip

Small repeating earthquakes occur on a number of faults and their observations have been used to study various aspects of earthquake physics and mechanics (e.g., Ellsworth and Dietz, 1990; Vidale et al., 1994; Marone et al., 1995; Nadeau and Johnson, 1998; Schaff et al., 1998; Nadeau and McEvilly, 1999, 2004; Bürgmann et al., 2000; Beeler et al., 2001; Sammis and Rice, 2001; Igarashi et al., 2003; Imanishi et al., 2004; Nadeau et al., 2004; Schaff and Beroza, 2004; Matsubara et al., 2005; Allmann and Shearer, 2007; Chen et al., 2007; Rubinstein et al., 2012).

We have continued our studies of small repeating earthquakes (which occur in the creeping segment close to the Parkfield segment) and properties of the creeping region that surrounds them. Such work informs our development of the combined model of the Parkfield and creeping segments, building on the Parkfield model by Barbot et al. (2012), which will be in part used to understand the potential for a large seismic event to propagate through the creeping segment.

Our studies of interaction between two repeating earthquake sequences (Lui and Lapusta, 2016; Figure 7) show that much of the interaction occurs through the stress changes transported by accelerated creep in the VS areas between the seismogenic patches. Hence one can determine the properties of the creeping areas based on the observed triggering time between the events in the two interacting sequences. In fact, our preliminary models of the SF and LA repeating sequences (SAFOD targets) and their interaction (Figure 8) indicate that velocity-strengthening properties of the creeping segment in that area are between 0.004 and 0.008 for the effective normal stress of 120 MPa, values consistent with laboratory measurements as well as prior estimates (Blanpied et. al., 1995; Johnson et. al., 2006; Barbot et al., 2009).

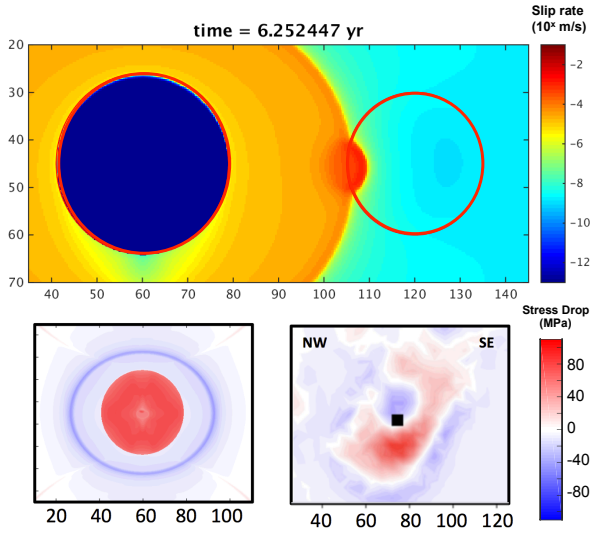

Figure 8. Simulations of the SF and LA repeating sequences. (Top) Slip-rate snapshot showing postseismic slip from a SF event triggering the LA patch. Red circles indicate the two VW patches. The left (SF) patch, which is now locked, has just experienced a seismic event. The (traveling) postseismic slip (orange) has just arrived at the LA patch, initiating near-seismic slip there (red). The LA patch ruptures next (not shown), with the time delay between the two seismic events being minutes, consistent with observations, for (a – b) of the VS area between 0.004 and 0.008. (Bottom) The simulated stress drop due to the SF event (left) and its comparison to the inferred stress drop from a finite-fault slip inversion based on the SAFOD data (Dreger et al., 2007). The values of the stress drop are similar, with peak values up to 90 MPa. The stress drop is positive inside the VW patch and negative outside. The average stress drop in our model is ~20 MPa, comparable to the average stress drop of ~30 MPa inferred by Abercrombie (2014). In our simulations, such a high value of stress drop is achieved by enhanced coseismic weakening. Compared to our numerical results, the observationally inferred stress drop distribution is much more heterogeneous. Hence our next step is to implement a heterogeneous model, in which each repeater occurs on a collection of closely spaced and/or intersecting patches.

REFERENCES

Abercrombie, R. E., Stress drops of repeating earthquakes on the San Andreas Fault at Parkfield, *Geophys. Res. Lett.*, **41**, doi: 10.1002/2014GL062079, 2014.

Allmann, B. P., and P. M. Shearer, Spatial and temporal stress drop variations in small earthquakes near Parkfield, California, *J. Geophys. Res*., **112**, B04305, doi:10.1029/2006JB004395, 2007.

Andrews, D. J., A fault constitutive relation accounting for thermal pressurization of pore fluid, *J. Geophys. Res*., **107**(B12), 2363, doi:10.1029/2002JB001942, 2002.

Barbot, S., Y. Fialko, and Y. Bock, Postseismic deformation due to the Mw 6.0 2004 Parkfield earthquake: stress-driven creep on a fault with spatially variable rate-and-state friction parameters, J. Geophys. Res., **114**, B07405, doi:10.1029/2008JB005748, 2009.

Barbot, S., N. Lapusta, and J.-P. Avouac, Under the hood of the earthquake machine: Toward predictive modeling of the seismic cycle, *Science*, *336*(6082), 707–710, doi:10.1126/science.1218796, 2012.

Beeler, N. M., D. L. Lockner, and S. H. Hickman, A simple stick-slip and creep-slip model for repeating earthquakes and its implication for microearthquakes at Parkfield, *Bull. Seismol. Soc. Am*., **91**, 1797–1804, 2001.

Beeler, N. M., and T. E. Tullis, Constitutive relationships for fault strength due to flash-heating. In: *2003 SCEC Annual Meeting Proceedings and Abstracts*, vol. 13, p. 66. Los, Angeles: Southern California Earthquake Center, Univ. of Southern California, 2003.

Beeler, N. M., T. E. Tullis, and D. L. Goldsby , Constitutive relationships and physical basis of fault strength due to flash-heating, *J. Geophys. Res*., **113**, B01401, doi:10.1029/2007JB004988, 2008.

Bizzarri, A., and M. Cocco, A thermal pressurization model for the spontaneous dynamic rupture propagation on a three-dimensional fault: 1. Methodological approach, *J. Geophys. Res*., **111**, B05303, doi:10.1029/2005JB003862, 2006a.

Bizzarri, A., and M. Cocco, A thermal pressurization model for the spontaneous dynamic rupture propagation on a three-dimensional fault: 2. Traction evolution and dynamic parameters, *J. Geophys. Res*., **111**, B05304, doi:10.1029/2005JB003864, 2006b.

Blanpied, M. L., D. A. Lockner and J. D. Byerlee, Fault stability inferred from granite sliding experiments at hydrothermal conditions, *Geophys. Res. Letters*, **18** (4), 609-612, 1991.

Blanpied, M. L., D. A. Lockner and J. D. Byerlee, Frictional slip of granite at hydrothermal conditions, *J. Geophys. Res*., **100**, 13045-13064, 1995.

Bouchon, M. & H. Karabulut, The aftershock signature of supershear earthquakes. Science 320, 1323–1325 (2008).Medline doi:10.1126/science.1155030.

Bürgmann, R., D. Schmidt, R. M. Nadeau, M. d'Alessio, E. Fielding, D. Manaker, T. V. McEvilly, and M. H. Murray, Earthquake potential along the northern Hayward fault, California, *Science*, **289**, 1178–1182, 2000.

Chen, K. H., Bürgmann, R., and Nadeau, R. M., Do repeating earthquakes talk to each other?, *EOS Trans. AGU*, S33C-1469, 2007.

Chen, T., and N. Lapusta , Scaling of small repeating earthquakes explained by interaction of seismic and aseismic slip in a rate and state fault model, *J. Geophys. Res.*, 114, B01311, doi:10.1029/2008JB005749, 2009.

Chen, T., and N. Lapusta, Interaction of small repeating earthquakes in a rate and state fault model, *AGU Fall Meeting*, T33B-2255, 2010.

Day, S. M., L. A. Dalguer, N. Lapusta, Y. Liu, Comparison of finite difference and boundary integral solutions to three-dimensional spontaneous rupture. J. Geophys. Res.110, B12307 (2005). doi:10.1029/2005JB003813

Dieterich, J. H., Modeling of rock friction- 1 Experimental results and constitutive equations, *J. Geophys. Res.*, **84**, 2161-2168, 1979.

Dieterich, J. H., Constitutive properties of faults with simulated gouge, in *Mech. Beh. Crustal Rocks*, Geophys. Monogr. Ser., **24**, ed. by N. L. Carter, M. Friedman, J. M. Logan and D. W. Stearns, AGU, Washington, DC, 103-120, 1981.

Dieterich, J. H. Applications of rate- and state-dependent friction to models of fault slip and earthquake occurrence. In Kanamori, H. (ed.) *Treatise on Geophysics*, **4**, chap. 4, 107–129 (Elsevier, Amsterdam, 2007).

Dreger, Douglas, Robert M. Nadeau, and Angela Chung. "Repeating earthquake finite source models: Strong asperities revealed on the San Andreas Fault." *Geophysical Research Letters* 34.23 (2007).

Ellsworth, W. L. and L. D. Dietz, Repeating earthquakes: characteristics and implications, Proc. of Workshop 46, the 7th U.S.-Japan Seminar on Earthquake prediction, U.S.Geol.Surv. Open-File Rept. 90-98, 226-245, 1990.

Fialko, Y., Interseismic strain accumulation and the earthquake potential on the southern San Andreas fault system. Nature 441, 968–971 (2006).Medline doi:10.1038/nature04797

Goldsby, D. L., and T. E. Tullis, Flash heating/melting phenomena for crustal rocks at (nearly) seismic slip rates. In: *2003 SCEC Annual Meeting Proceedings and Abstracts*, vol. 13, p. 98-99. Los Angeles: Southern California Earthquake Center, Univ. of Southern California, 2003.

Grant, L. B., A. Donnellan, 1855 and 1991 surveys of the San Andreas fault: Implications for fault mechanics. Bull. Seismol. Soc. Am.84, 241–246 (1994).

Hauksson, E., W.Yang, P. M. Shearer, Waveform relocated earthquake catalog for southern California (1981 to June 2011). Bull. Seismol. Soc. Am. 102, 2239–2244 (2012). doi:10.1785/0120120010.

Igarashi, T., Matsuzawa, T., and A. Hasegawa, Repeating earthquakes and interplate aseismic slip in the northeastern Japan subduction zone, *J. Geophys. Res.* 108, B5, 2249, 2003.

Imanishi, K., W. L. Ellsworth, S. G. Prejean, Earthquake source parameters determined by the SAFOD Pilot Hole seismic array, *Geophys. Res. Letters*, **31**, L12S09, doi:10.1029/2004GL019420, 2004.

Jiang, J., and N. Lapusta, Deeper penetration of large earthquakes on seismically quiescent faults, *Science*, 352, 2016.

Jiang, J., and N. Lapusta, Connecting depths of seismicity, fault locking, and coseismic slip using long-term fault models, *AGU Fall Meeting*, San Francisco, CA, Dec. 2015. (Oral presentation)

Jiang, J., and N. Lapusta, Connecting depths of seismicity, fault locking, and coseismic slip using long-term fault models, *SCEC Annual Meeting*, Palm Springs, CA, Sept. 2015.

Jiang, J., and N. Lapusta, Variability of earthquake slip and arresting depth in fault models with depth-dependent properties, *SSA Annual Meeting*, Pasadena, CA, Apr. 2015.

Johnson, K. M., R. Bürgmann, and K. Larson, Frictional properties on the San Andreas fault near Parkfield, California, inferred from models of afterslip following the 2004 earthquake, *Bull. Seism. Soc. Am.,* 96, 4B, S321-S338, 2006.

Lapusta, N., and Y. Liu, 3D boundary-integral modeling of spontaneous earthquake sequences and aseismic slip, accepted for publication, *J. Geophys. Res.*, 2009.

Lapusta, N., J. R. Rice, Y. Ben-Zion, and G. Zheng, Elastodynamic analysis for slow tectonic loading with spontaneous rupture episodes on faults with rate- and state-dependent friction, *J. Geophys. Res*. 105, 23765-23789, 2000.

Lapusta, N. and J. Jiang, Long-term fault slip in models with depth-dependent permeability and shear zone width: depth extent and spatio-temporal complexity of earthquake ruptures, *AGU Fall Meeting*, San Francisco, CA, Dec. 2014. (Invited oral presentation)

Lui, S.K.Y., and N. Lapusta, Repeating microearthquake sequences interact predominantly through postseismic slip, *Nature Comm*, doi: 10.1038/ncomms13020, 2016.

Marone, C., Vidale, J. E., and W. L. Ellsworth, Fault healing inferred from time-dependent variations in-source properties of repeating earthquakes, *Geophys. Res. Lett.,* 22, 3095-3098, 1995.

Matsubara, M., Y. Yagi, and K. Obara, Plate boundary slip associated with the 2003 off-Tokachi earthquake based on small repeating earthquake data, *Geophys. Res. Lett*., **32**, L08316, doi:10.1029/2004GL022310, 2005.

Mizoguchi, K., T. Hirose, T. Shimamoto, E. Fukuyama, Internal structure and permeability of the Nojima fault, southwest Japan. J. Struct. Geol.30, 513–524 (2008). 10.1016/j.jsg.2007.12.002 doi:10.1016/j.jsg.2007.12.002.

Nadeau, R. M., and L. R. Johnson, Seismological studies at Parkfield VI: Moment release rates and estimates of source parameters for small repeating earthquakes, *Bull. Seism. Soc. Am.,* 88, 1998.

Nadeau, R. M., and T. V. McEvilly, Fault slip rates at depth from recurrence intervals of repeating microearthquakes, *Science*, **285**, 718–721, 1999.

Nadeau, R. M., and T, V. McEvilly, Periodic Pulsing of Characteristic Microearthquakes on the San Andreas Fault, *Science*, 303, 220-223, 2004.

Nadeau, R. M., A. Michelini, R. A. Uhrhammer, D. Dolenc, T. V. McEvilly, Detailed kinematics, structure and recurrence of micro-seismicity in the SAFOD target region, *Geophys. Res. Letters*, **31**, L12S08, doi:10.1029/2003GL019409, 2004.

Noda, H. "Numerical simulation of rupture propagation with thermal pressurization based on measured hydraulic properties: Importance of deformation zone width." *AGU Fall Meeting Abstracts*. 2004.

Noda, H., E. M. Dunham, and J. R. Rice, Earthquake ruptures with thermal weakening and the operation of major faults at low overall stress levels, *J. Geophys. Res.*, *114*, B07302, doi:10.1029/2008JB006143, 2009.

Noda, H., and N. Lapusta, Three-dimensional earthquake sequence simulations with evolving temperature and pore pressure due to shear heating: Effect of heterogeneous hydraulic diffusivity, *J. Geophys. Res.*, *115*(B12), doi:10.1029/2010JB007780, 2010.

Noda, H., and N. Lapusta, Stable creeping fault segments can become destructive as a result of dynamic weakening, *Nature*, 1–6, doi:10.1038/nature11703, 2013.

Reilinger, R. E., S. Ergintav, R. Bürgmann, S. McClusky, O. Lenk, A. Barka, O. Gurkan, L. Hearn, K. L. Feigl, R. Cakmak, B. Aktug, H. Ozener, M. N. Töksoz, Coseismic and postseismic fault slip for the 17 August 1999, M = 7.5, Izmit, Turkey earthquake. Science 289, 1519–1524 (2000). Medline doi:10.1126/science.289.5484.1519

Rice, J. R. "Flash heating at asperity contacts and rate-dependent friction." *Eos Trans. AGU* 80.46 (1999): F471.

Rice, J. R., Heating and weakening of faults during earthquake slip, *J. Geophys. Res.*, doi:10.1029/2005JB004006, 2006.

Rice, J. R., N. Lapusta, and K. Ranjith, Rate and state dependent friction and the stability of sliding between elastically deformable solids, *J. Mech. Phys. Solids* 49, 1865-1898, 2001.

Rubinstein, J. L., and G. C. Beroza, Full waveform earthquake location: Application to seismic streaks on the Calaveras Fault, California, *J. Geophys. Res.*, *112*(B5), doi:10.1029/2006JB004463, 2007.

Rubinstein, J.L., W.L. Ellsworth, K.H. Chen, and N. Uchida, The time and slip-predictable models cannot be dependably used to predict earthquake behavior 1: Repeating earthquakes, *J. Geophys. Res.,*117, B02306, doi:10.1029/2011JB008724, 2012.

Ruina, A. L., Slip instability and state variable friction laws, *J. Geophys. Res*., **88**, 10359-10370, 1983.

Sammis, C. G., and J. R. Rice, Repeating earthquakes as low-stress-drop events at a border between locked and creeping fault patches, *Bull. Seism. Soc. Am.,* 91, 3, 532-537, 2001.

Schaff, D. P., G. C. Beroza, and B. E. Shaw, Postseismic response of repeating aftershocks, *Geophys. Res. Lett*., **25**, 4549– 4552, 1998.

Schaff, D. P., and G. C. Beroza, Coseismic and postseismic velocity changes measured by repeating earthquakes, *J. Geophys. Res*., **109**, B10302, doi:10.1029/2004JB003011, 2004.

Scholz, C. H. Earthquakes and friction laws. *Nature* **391**, 37–42, 1998.

Sibson, R. H., Interaction between temperature and pore-fluid pressure during earthquake faulting and a mechanism for partial or total stress relief, *Nature*, **243**, 66–68, 1973.

Sieh, K. E., Slip along the San Andreas fault associated with the great 1857 earthquake. Bull. Seismol. Soc. Am.68, 1421–1434 (1978).

Shaw, B. E., and S. G. Wesnousky, Slip-Length Scaling in Large Earthquakes: The Role of Deep-Penetrating Slip below the Seismogenic Layer, *Bull. Seismol. Soc. Amer.*, *98*(4), 1633–1641, doi:10.1785/0120070191, 2008.

Smith-Konter, B. R., D. T.Sandwell, P. M. Shearer, Locking depths estimated from geodesy and seismology along the San Andreas Fault System: Implications for seismic moment release. J. Geophys. Res.116, B06401 (2011). doi:10.1029/2010JB008117

Tanikawa, W. & Shimamoto, T. Frictional and transport properties of the Chelungpu fault from shallow borehole data and their correlation with seismic behavior during the 1999 Chi-Chi earthquake. *J. Geophys. Res.* **114**, B01502, doi:10.1029/2008JB005750, 2009.

Tsutsumi, A. & Shimamoto, T. High velocity frictional properties of gabbro. *Geophys. Res. Lett.* **24**, 699–702, 1997.

Tullis, T., Mechanisms for friction of rock at earthquake slip rates, in Treatise on Geophysics, G. Schubert, Ed. (Elsevier, Oxford, ed. 2, 2007), vol. 4, chap. 6, pp. 139–159.

Vidale, J. E., Ellsworth, W. L., Cole, A., and C. Marone, Variations in rupture process with recurrence interval in a repeated small earthquake, *Nature*, 368, 6472, 624-626, 1994.

Waldhauser, F., W. L. Ellsworth, D. P. Schaff, and A. Cole, Streaks, multiplets, and holes: High-resolution spatio-temporal behavior of Parkfield seismicity, *Geophys. Res. Lett.*, doi:10.1029/2004GL020649, 2004.

Zielke, O., J. R. Arrowsmith, L. G . Ludwig, S. O. Akçiz, Slip in the 1857 and earlier large earthquakes along the Carrizo Plain, San Andreas Fault. Science 327, 1119–1122 (2010). Medline doi:10.1126/science.1182781